Pertanika J. Sci. & Technol. 30 (4): 2613 - 2638 (2022)

PERTANIKA JOURNALS

SCIENCE & TECHNOLOGY

Journal homepage: http://www.pertanika.upm.edu.my/

ZnO Multilayer Thin Films as the Seed Layer for ZnO Nanorods: Morphology, Structural and Optical properties

Rohanieza Abdul Rahman[1,2], Muhammad AlHadi Zulkefle[1,2], Sukreen Hana Herman[1,3]* and Rosalena Irma Alip[1,4]

[1]*Integrated Sensors Research Group, School of Electrical Engineering, College of Engineering, Universiti Teknologi MARA, 40450 UiTM, Shah Alam, Selangor, Malaysia*
[2]*NANO-Electronic Centre, School of Electrical Engineering, College of Engineering, Universiti Teknologi MARA, 40450 UiTM, Shah Alam, Selangor, Malaysia*
[3]*Microwave Research Institute (MRI), Universiti Teknologi MARA, 40450 UiTM, Shah Alam, Selangor, Malaysia*
[4]*Terahertz Sensing and Research Team, RIKEN Center for Advanced Photonics, RIKEN, Sendai, Japan*

ABSTRACT

The effect of zinc oxide (ZnO) multilayer thin film thicknesses, deposited via the sol-gel spin coating technique, on the morphology, structural and optical properties of ZnO nanorods (ZNR) grown on the ZnO thin films were explored in this investigation. The ZNR was grown using the chemical bath deposition method on the ZnO thin film seed layer (SL). We found that ZnO thin film SL morphology changes according to the number of layers based on the results. Eventually, these changes also influence the structures of ZNR. ZNR structures improved when the thickness of the seed layer increased. Besides the surface roughness, better crystalline quality films were obtained when more layers were deposited. This crystalline quality then influenced the optical characteristics of both ZnO and ZNR thin films. The optical properties from UV-Vis showed transmittance in the visible region, showing that the ZnO films produced were suitable to be applied to solar cells. ZNR-based solar cells have become one of the promising materials to be studied further due to the environment-friendly, low-cost, and well-abundant material for solar cell applications.

ARTICLE INFO

Article history:
Received: 07 October 2021
Accepted: 02 March 2022
Published: 21 September 2022

DOI: https://doi.org/10.47836/pjst.30.4.18

E-mail addresses:
rohanieza.abdrahman@gmail.com (Rohanieza Abdul Rahman)
alhadizulkefle@gmail.com (Muhammad AlHadi Zulkefle)
hana1617@uitm.edu.my (Sukreen Hana Herman)
rosalena@uitm.edu.my (Rosalena Irma Alip)
* Corresponding author

Keywords: Chemical bath deposition, crystallinity, nanorods, seed layer, solar cells, sol-gel, spin coating

INTRODUCTION

Zinc oxide (ZnO) is classified as an n-type semiconductor that could be found abundantly. ZnO is classified in II-VI semiconductors and has become favorable

ISSN: 0128-7680
e-ISSN: 2231-8526

among researchers because it owns a wide band gap (3.2–3.4 eV) and is also low-cost and non-toxic. These characteristics have left it within the detectable region that possesses high optical transmission, sufficient for the basic range sun detection (Rwenyagila et al., 2014). Therefore, it has wide applications in optoelectronic devices due to its electrical, structural, and optical properties (Khan et al., 2021; Sharma et al., 2014; Djurisic et al., 2010). Besides, ZnO also possesses numerous families of nanostructures. Numerous studies show that ZnO could be synthesized to produce nanoring, nanobelts, nanowires, and nanorods (Alenezi et al., 2018; Chen et al., 2021; Mohammadzadeh et al., 2020).

Nanorods are one of the ZnO nanostructures that have been greatly explored by many researchers (Huey et al., 2021; Kannan et al., 2020; Zhou et al., 2019). ZnO nanorods (ZNR) are 1-dimensional (1D) nanostructures with fascinating physical properties. Moreover, 1D structures like ZNR are believed to have more surface-to-volume ratio than 2-dimensional (2D) structures; thus, this type of nanostructures offers an enhancement to increase the sensitivity in many applications (Zhang et al., 2012). Various methods could be utilized to grow ZNR, such as vapor-liquid-solid (VLS), physical vapor deposition (PVD), pulse laser deposition (PLD), chemical vapor deposition (CVD), and the most favorable approach among researchers is chemical bath deposition (CBD) (Kumar et al., 2018; Jimenez-Cadena et al., 2010; Hajezi et al., 2008; Rodriguez-Martinez et al., 2020; Mosalagae et al., 2020). CBD is a favorable method to synthesize ZNR owing to the ability to produce good crystallinity quality films, aside from the low cost and low-temperature process. Many researchers are actively studied in controlling the morphology and structures of ZNR using this CBD method (Roy et al., 2013; Khranovskyv et al., 2012; Abdulrahman et al., 2020). Many reported studies to show that vital parameters could control the growth of ZNR, such as growth temperature and duration, type of SL, precursor concentration, pH of the aqueous solution, and thickness of SL (Abdulrahman et al., 2020).

Considering all these essential considerations, the SL becomes an important element in controlling the growth of ZNR. Hence, the SL's thickness is influential in producing a well-aligned ZNR. A few approaches controlled this thickness. One of the approaches considered is depositing a multilayer of SL during the deposition process.

Multilayer or layer by layer ZnO can be produced or deposited by many methods. The method of deposition includes RF magnetron sputtering, pulse laser deposition (PLD), spray pyrolysis, dip-coating, and sol-gel spin coating techniques (Hasabeldaim et al., 2020; Al Farsi et al., 2021; Regmi & Velumani, 2021; Abdel-Galil et al., 2021; Lokesh et al., 2020). Advantages such as simple, practical in terms of cost, and large area deposition technique make sol-gel spin coating favorable among researchers. According to the previous research and findings, it is important to determine a suitable thickness for the SL since it can be an essential factor in producing well-aligned ZNR (Banari et al., 2021). Well-aligned ZNR offers more effective performance in many applications. For example, Gunes et al. (2007)

stated that aligned ZnO nanorods are employed in solar cell applications to raise the persistence of the cell. In addition, the movement of the charge carrier was also regulated by the tidy rods that were constructed by well-aligned nanorods. Based on this, the suitable thickness of the ZnO SL needs to be controlled to produce a well-aligned ZNR. In this investigation, multilayer ZnO thin films were deposited layer by layer via the sol-gel spin coating technique to obtain a suitable thickness for ZnO thin film that functions as the SL for ZNR. One to five layers of ZnO were deposited, and these prepared ZnO thin films were applied as the SL to grow ZNR by the CBD method. All ZnO and ZNR films were characterized morphologically, structurally, and optically to study the impact of the SL thickness on the ZNR properties.

METHODOLOGY

This study can be separated into two different parts. The first part is the deposition of ZnO thin films with different layers, followed by the growth of ZNR on five different numbers SL. Then, after the fabrication process of ZnO and ZNR thin films was performed, the characterization process for physical, structural, and optical properties was carried out. All these processes are explained in the next subsections. Finally, the summary of the overall methodology is illustrated in Figure 1.

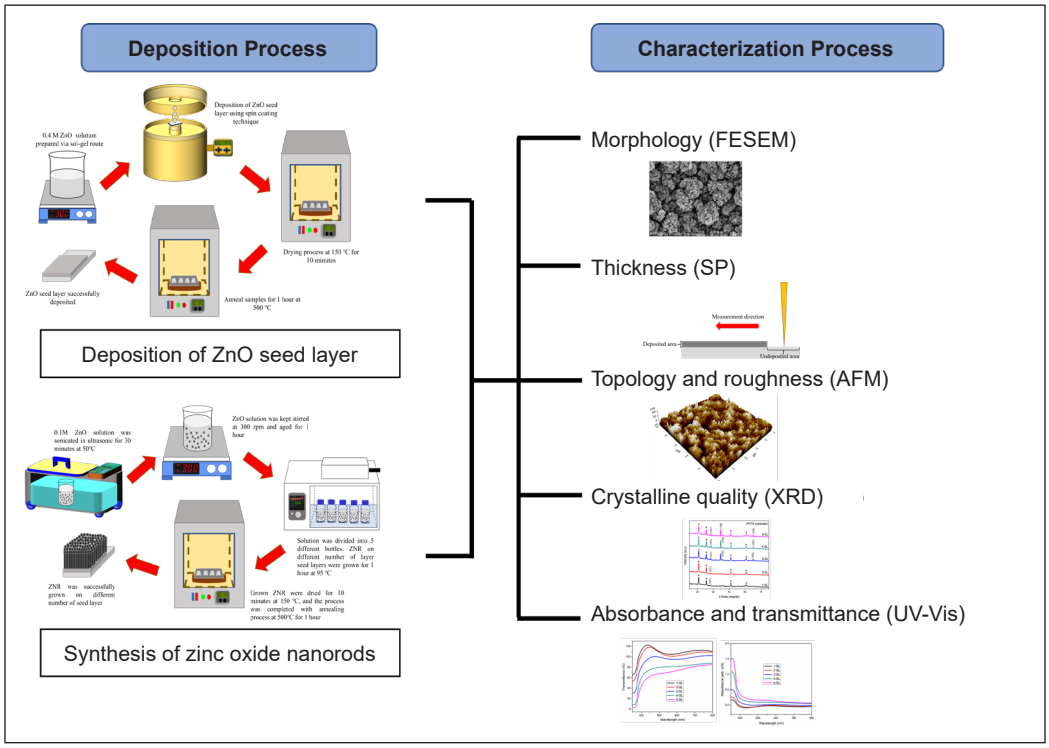

Figure 1. Summary of deposition and characterization process

Deposition of ZnO Thin Films by Sol-Gel Spin Coating Technique

0.4M ZnO solution was produced via the sol-gel method by mixing the following chemicals: zinc acetate anhydrate, monoethanolamine (MEA), and 2-methoxyethanol. For the precursor, zinc acetate anhydrate was used, while MEA acted as the stabilizer, and for the solvent, 2-methoxyethanol was employed. At first, zinc acetate was weighed and put in a Schott bottle. 2.4 mL of MEA was poured into the bottle before 2-methoxyethanol was added until the total solution was 100 mL. This mixture was stirred on a hot plate at 300 rpm with 80 °C heat. The heat was switched off after 3 hours, and the stirring process continued as the aging process for 24 hours to produce a homogenous and transparent (clear) 0.4M ZnO solution.

The deposition process was performed via the spin-coating technique when the aging process was completed. ZnO thin film had been deposited with different numbers of SL. This investigation employed indium tin oxide (ITO) as a substrate. Beforehand, ITO substrates were cleaned using a standard cleaning process, using ethanol and deionized water (DI). The spin-coating process started by placing the ITO substrate on the stage of the spin-coater (center), then ZnO solution (10 drops) was dropped onto the spinning substrate. This spinning process was set up at 3000 rpm for 60 seconds. After that, the deposited sample was let dry in a furnace at 150°C for ten minutes. These processes were repeated to obtain ZnO thin films with 1, 2, 3, 4, and 5 layers. Each layer was dried after being deposited with ZnO solution. Finally, the annealing process was carried out for one hour, at 500°C, after the last layer was deposited to complete the deposition process. Figure 2 shows the experimental diagram for ZnO thin film deposition process, while Table 1 describes the classification of the samples produced in this investigation.

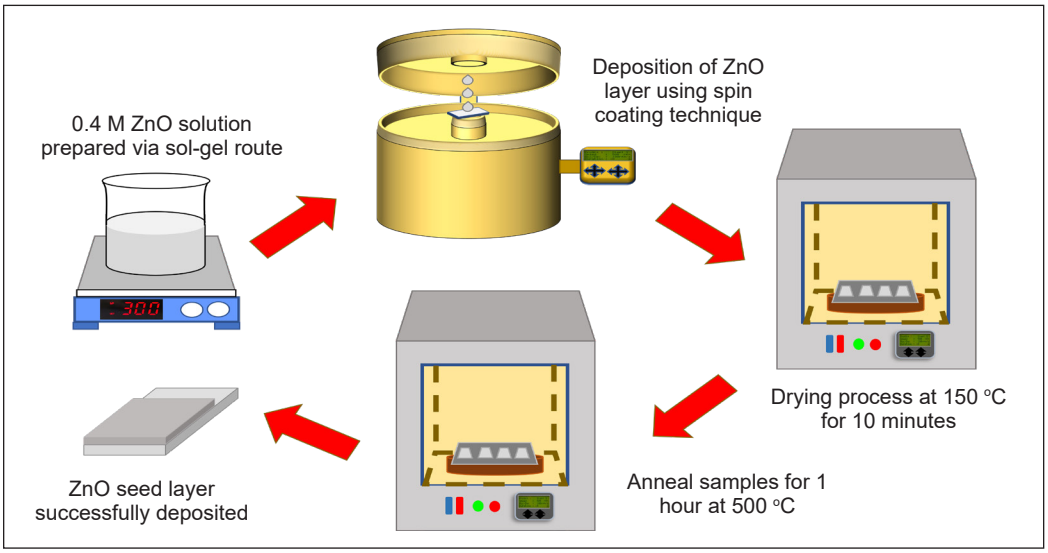

Figure 2. Sol-gel spin coating process for ZnO thin films samples with different number of layers

Table 1
Classification for ZnO samples produced

Number of deposition layer	1	2	3	4	5
Classification	1-SL	2-SL	3-SL	4-SL	5-SL

Growth of Zinc Oxide Nanorods via Chemical Bath Deposition Method

A 0.1M ZnO solution was first prepared by dissolving zinc nitrate hexahydrate ($Zn(NO_3)_2 \cdot 6H_2O$, 99%) and hexamethylenetetramine ($(CH_2)6N_4$, 99.5%) in deionized water (DI) to grow ZNR. Then, the molar ratio of $Zn(NO_3)_2 \cdot 6H_2O$ and $(CH_2)6N_4$ was fixed to 1:1, and DI water was poured into the used beaker to get 500 mL of ZnO solution. The sonication process was the next step using an ultrasonic bath (Hwasin Technology PowerSonic 405, 40 kHz). ZnO solution was sonicated at 50 °C for 30 minutes. After that, the solution was kept stirred on a hot plate at 300 rpm for 1 hour at room temperature. When the aging process was completed, the prepared ZnO solution was divided into five different Schott bottles, with 100 mL volume each. ZnO thin films with the different number of layers deposited earlier were immersed upside down in each Schott bottle.

Then, all these bottles were put into a hot bath (Memmert) that contained preheated DI water. The hot bath temperature was set to 95 °C, and this growth process was fixed to one hour. After one hour, all the samples were taken out of the hot bath. These samples were first rinsed with DI water to eliminate the precipitate powder before drying at 150 °C for 10 minutes. Finally, the annealing process was performed for one hour at 500 °C to complete the growing process of ZNR. In summary, these processes are illustrated in Figure 3. The chemical in Equations 1 to 5 described the growth mechanism of ZnO nanorods.

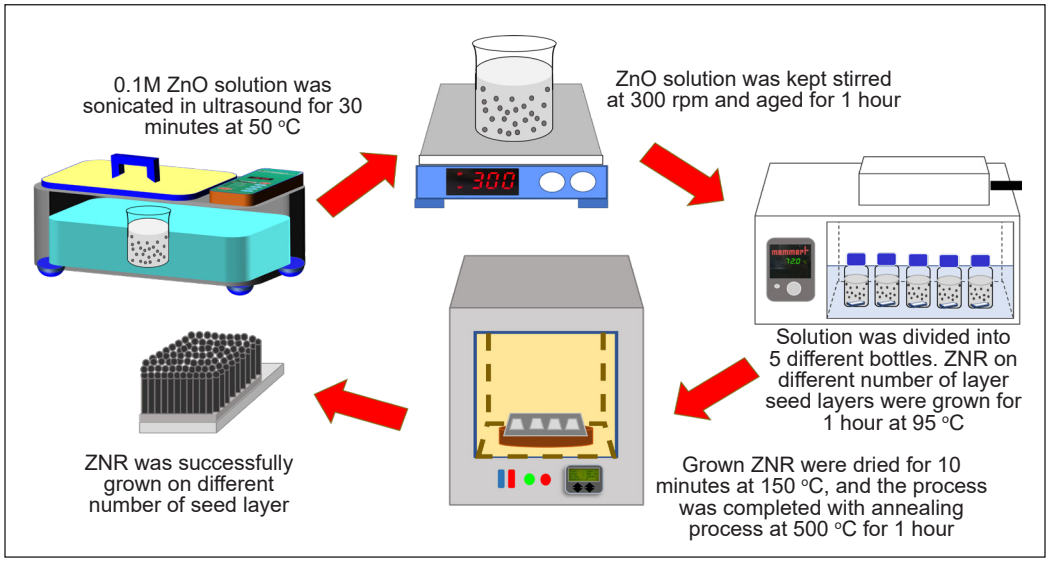

Figure 3. The growing process of ZNR by chemical bath deposition

$$Zn(NO_3)_2 + C_6H_{12}N_4 \leftrightarrow [Zn(C_6H_{12}N_4)^{2+} + 2NO^{3-} \quad [1]$$

$$C_6H_{12}N_4 + 4H_2O \leftrightarrow C_6H_{12}N^{4+} + 4OH^- \quad [2]$$

$$[Zn(C_6H_{12}N_4)]^{2+} + 4OH^- \leftrightarrow Zn(OH)_4^{2-} + C_6H_{12}N_4 \quad [3]$$

$$Zn(OH)_4^{2-} \rightarrow Zn(OH)_2 + 2OH^- \quad [4]$$

$$ZnO(OH)_2 \leftrightarrow ZnO + H_2O \quad [5]$$

Characterization of ZnO and ZNR Thin Film

All the deposited ZnO and ZNR thin films were characterized to examine their physical, optical, and structural properties. Morphological of ZnO and ZNR were explored by field emission scanning electron microscope (FESEM, Hitachi SU-030), while the optical properties were explored with an ultraviolet-visible spectrometer (UV-Vis, Jasco/V-670 EX). A surface profilometer (SP, KLA-Tencor P-6 Stylus Profiler) was chosen to measure the thickness of all samples in this study. An atomic force microscope (AFM, Park Systems XE-100) characterized the surface topology and the roughness of thin films. The characterization was performed using X-ray diffraction (XRD, PANalytical X'Pert PRO) to determine all samples' crystallinity quality (structural properties). The results obtained from these characterizations are present and discussed in the next section.

RESULTS AND DISCUSSION

Morphology of ZnO thin films deposited with the different number of layers was observed using FESEM. Figure 4 presents the images obtained for ZnO thin film deposited with 1 and 5 layers. A contrast change could be identified in Figures 4(a) and (b), in which the structures of ZnO thin films become denser and uniform when further layers are deposited. Even though 1-layer ZnO thin film shows a uniform structure, small cracks could be observed. These cracks improved the increased number of deposition layers. Crack-free and clear agglomeration structure was shown in Figure 4(b), proving that several layers produce a better structure of ZnO thin films. The difference between these structures might be from the spin-coating process. The uniformity of a thin film could be affected by the spin-coating process.

In contrast, in a 1-layer ZnO thin film, the distribution of ZnO nanoparticles was not evenly spread, thus producing less uniform ZnO structures. Increasing the deposition layer could overcome this issue. The non-uniform ZnO nanoparticles were then covered by the subsequent layers of ZnO nanoparticles, which resulted in a more uniform structure of ZnO thin film. the uncovered area was covered by the next layer of ZnO deposition during the first layer, resulting in better and uniform structures. This statement was supported

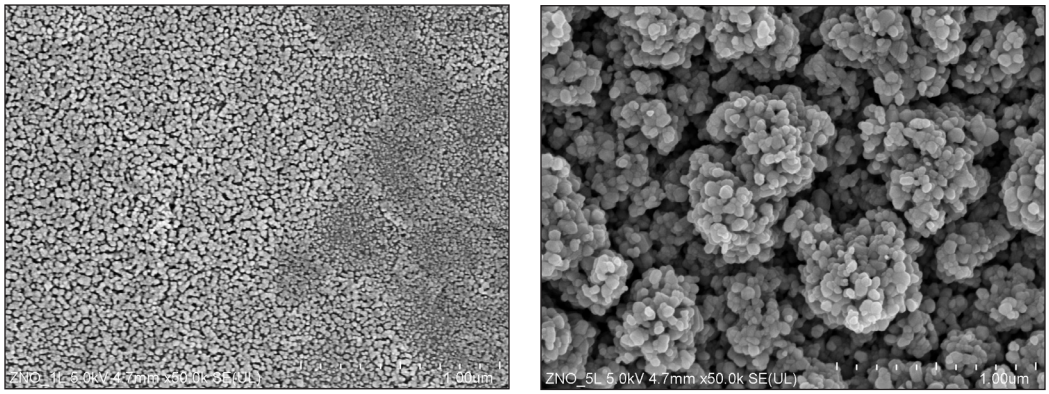

(a) (b)

Figure 4. Comparison of ZnO thin films deposited with (a) 1-layer and (b) 5-layers

by the FESEM images in Figure 4(b), in which an improvement of ZnO nanostructures was achieved when the number of layers was increased. This finding indicates that good quality ZnO thin films (dense and crack-free) could be produced with the increment of deposition layers.

In a study reported by Kumar et al. (2013), the same parameter was varied. However, the thickness for each layer was constantly deposited, which is ~19 nm. According to their findings, the morphology and structure of their ZnO thin films were improved as the number of depositions was increased (Kumar et al., 2013). It is due to the thickness increment of the thin films when further layers are deposited. Based on their study, Kumar et al. (2013) also stated that thicker film produces better morphology of ZnO thin films. Similar to this study, particles in the 5-layer ZnO thin film show a higher thickness, correlated with the increase in the number of layers, compared with the 1-layer ZnO thin film. This statement is proven by the surface profilometer (SP) measurement. The thickness of the samples significantly changes with the number of layers. Table 2 describes the thickness value for all samples deposited with different layers.

Table 2
The value of thickness ZnO thin films deposited with variation layers

Sample	**1-SL**	**2-SL**	**3-SL**	**4-SL**	**5-SL**
Film thickness (nm)	58.52	123.23	195.03	236.85	284.20

Table 2 shows the thickness values for each ZnO thin film deposited with a different number of layers. Based on the results, the thickness of the samples shows a proportional relationship with the number of deposition layers. Significant changes could be seen in each sample. As shown in Table 2, an almost constant value was found when each layer was deposited on the existing ZnO layer. An average value of ~56 nm was determined

based on the measured data. This finding proved that the addition of each layer contributes to the increasing thickness trend of ZnO thin films with a different number of layers. This occurrence might come from the amount of ZnO nanoparticles that rise accordingly with the deposition layer. A higher number of layers provide many ZnO nanoparticles settling on the substrate or existing layer of ZnO (Khan et al., 2017). Hence, a higher value of thickness is produced. This attained result can be related to the finding reported by Shariffudin et al. (2012) in which ZnO thin films in their study had higher thickness when several layers were added. They varied the number of layers during the spin-coating process, the thickness of the films changed, and the grain size for ZnO nanoparticles (Shariffudin et al., 2012).

Other than that, since the total thickness of ZnO thin film deposited with 5-layers is almost five times that of a 1-layer sample, we attribute this linear increment of the thickness to the drying process that we conducted at the end of each layer during the deposition process. The drying process improved and allowed the particles in one layer to be stable and dense before the subsequent layer was deposited. Regarding this drying process, Addamo et al. (2008) stated that when each layer was dried, the layer would grow over irregular and preformed the crystalline surface or structure, resulting in higher thickness for the films. It was based on their finding that they acquired thicker films when every layer was dried before the next layer was deposited. Besides, the increment of the thin film's thickness had influenced the surface topology and roughness of the ZnO thin films. It was proven by the results obtained from AFM measurement, as shown in Figure 5.

Figures 5(a) to 5(e) presented the 3-dimensional (3-D) images of ZnO thin films deposited for this study. The images indicate that the addition of the layer on top of the previous layer had affected the topology of the sample and the surface roughness. It could be observed that the roughness of the ZnO thin films increased with the addition of the number of layers, as the last sample with the highest thickness possesses the roughest surface. According to the AFM analysis, the surface roughness for all samples was recorded in the range of 4.77~9.20 nm, respectively. The rising surface roughness might be attributed to the formation of the grains that becomes larger significantly with the changes in thickness (Kumar et al., 2013). Besides, the correlation between the thickness of thin films and the film's roughness was also investigated by Kaiyong et al. (2005) and Daniel et al. (2014). Their studies concluded that roughness varies with thickness, where when thin films become thick, the film roughness increases. It corresponds with the findings in this study. This finding could be related to the agglomeration of the samples, which influenced the surface roughness of the thin films. Since the number of layers was increased, the total amount of available ZnO particles also increased. The ZnO particles then agglomerate, making the surface rougher.

The crystalline quality of the samples was influenced by the difference in the thickness value in this study. Figure 6 revealed the XRD spectra for all samples with different numbers of the deposition layer.

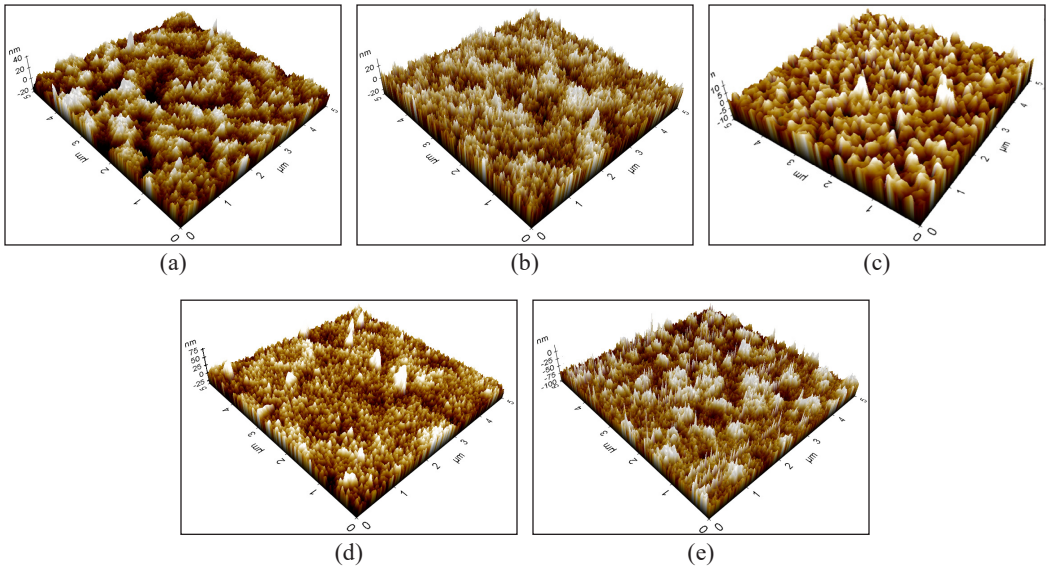

Figure 5. Surface topology of ZnO thin films with different number of deposition layers

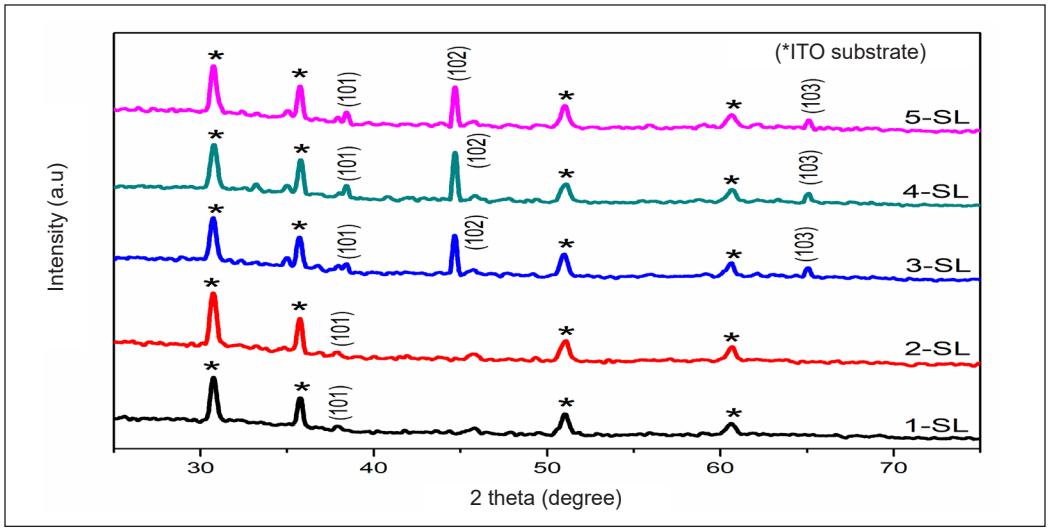

Figure 6. XRD analysis for all thin films deposited with different number of layers

The XRD patterns for all ZnO deposited with different layers are shown in Figure 6. Referring to the XRD pattern obtained, it is clearly shown that all deposited films are in good concurrence with the standard ZnO diffraction pattern of JCPDS no 36-1451. Referring to the XRD spectra, the diffraction peaks 2θ of ~37-38°, ~44.69°, and 65.11°, which correspond to (101), (102), and (103) crystalline peaks of ZnO, were observed. It could be seen that (101) peaks appear in all samples (1–5 layers). However, the intensity increment can be detected when further layers are deposited. The intensity increased in

the 3-SL sample and became higher at 4 and 5-SL. This (101) also shifted to the right due to improved crystalline quality. Meanwhile, (102) and (103) peaks are only present in 3, 4, and 5-SL ZnO thin films. Both peaks could not be observed in 1 and 2-SL samples but started to appear when ZnO thin film was deposited with three layers.

Among all peaks, (102) becomes dominant, and the highest intensity can be seen in 5-SL ZnO thin films. This result might be attributed to the thickness of the thin films that increase proportionally with the number of layers. The thicker film has more atomic layer to diffract X-rays (Goncalves et al., 2017). For the changes in the crystal orientation, we assume that as the layer increases, more atoms somehow tend to align in the (102) direction and pass the crystallographic information to the subsequent layers. The drying process conducted at each layer also might influence the crystalline quality of ZnO thin films. During the first layer deposition, the ZnO thin films were randomly oriented (Shariffudin et al., 2012). After the layer was dried, the stabilizer and solution vaporized. Then, after the deposition of the second layer, the first layer becomes a shape or template for the next layer, thus supporting the orientation and enhancing the crystalline properties of the deposited samples. With sufficient thickness and the number of layers, the peak and orientation become dominant compared to other peaks. On the other hand, the annealing process at the end of the deposition process also plays a crucial part in enhancing the crystallinity quality of the ZnO thin films.

Details of crystal properties for each of the peaks appearing in all samples are summarized in Table 3. The full width at half maximum (FWHM), crystallite size, *d*, dislocation line density, δ and interplanar spacing, *d*, values are tubulated based on the peaks obtained. Crystallite sizes were calculated using Scherer's formula, according to Equation 6.

$$d = \frac{0.94\lambda}{\beta \cos\theta} \quad [6]$$

d is the crystallite size for the samples, obtained according to the crystallographic peaks in XRD spectra, λ is the X-ray wavelength (1.542 Å), β is the diffraction line broadening/ expanding at half of the maximum intensity (FWHM) of the peak, and θ is the Bragg's angle of diffraction in radian (obtained from 2θ). From the determination of *d*, dislocation line density could be calculated using Equation 7, and interplanar spacing, *d,* for all peaks was determined using Equation 8

$$\delta = \frac{1}{d^2} \quad [7]$$

$$d = \frac{n\lambda}{2 \sin\theta} \quad [8]$$

According to Equation 7, dislocation line density was obtained by dividing 1 with the value of crystallite size, calculated using Equation 6. *d* in Equation 7 referring to the value of calculated crystallize size. For interplanar spacing, *d, n=1* is the order value of diffraction, while λ is the same value used in Equation 6, which is the X-ray wavelength (1.542 Å), and θ is the Bragg's angle of diffraction, which is the same value used for d calculation. An inversely proportional relationship between FWHM for all existence peaks with several layers could be observed in Table 3. Unlike FWHM, as described in Table 3, the crystallite size for ZnO thin films directly correlates with the number of layers. The value of crystallite size increase with the increment of the number of deposition layer. These findings are similar to the studies reported by Khan et al. (2017) and Kamalianfar et al. (2013). Both researchers also obtained the same finding, which the crystallite size for their ZnO thin films increased when they increased the number of layers throughout the deposition of the thin films. According to this, it is proven that the thickness had influenced the deposited samples' crystalline quality.

Table 3
Detail crystal properties for ZnO thin films deposited with 1, 2, 3, 4 and 5-layers

Sample	Orientation, hkl	2θ (°)	FWHM	Crystallite size, D (nm)	Dislocation line density, δ (δ x 10-3 line/nm2)	Interplanar spacing, d (Åm)
1-SL	101	37.96	0.5284	27.96	1.279	2.3705
2-SL	101	37.96	0.4874	30.32	1.088	2.3705
	101	38.47	0.3654	40.44	0.612	2.3403
3-SL	102	44.68	0.3113	47.47	0.438	2.0284
	103	65.11	0.3504	42.17	0.562	1.4329
	101	38.48	0.3638	40.62	0.606	2.3397
4-SL	102	44.68	0.3087	47.86	0.437	2.0284
	103	65.11	0.3449	42.84	0.545	1.4328
	101	38.48	0.3552	41.60	0.578	2.3397
5-SL	102	44.68	0.3066	48.19	0.431	2.0284
	103	65.23	0.3059	48.31	0.428	1.4303

Kamalianfar et al. (2013) also stated that the thickness or thicker film would give better crystallinity quality because thicker film tends to have a smaller value of dislocation line density, δ. The results obtained in this study agree with this statement, where the dislocation line density and δ value decline with the increment of the crystallize size and number of layers. Decreasing the value of δ means that the film has less dislocation of atom arrangement, thus improving the crystalline properties of the samples produced. As for the interplanar spacing, *d,* the value decreases as the peak appears at a higher degree (2θ). It is due to the increase of *hkl*, which is (101), (102), and (103). The increase of the *hkl* value produced a smaller value of interplanar spacing for each peak present (Bindu et al., 2014). Other than that, it could be observed that the interplanar spacing decrease with

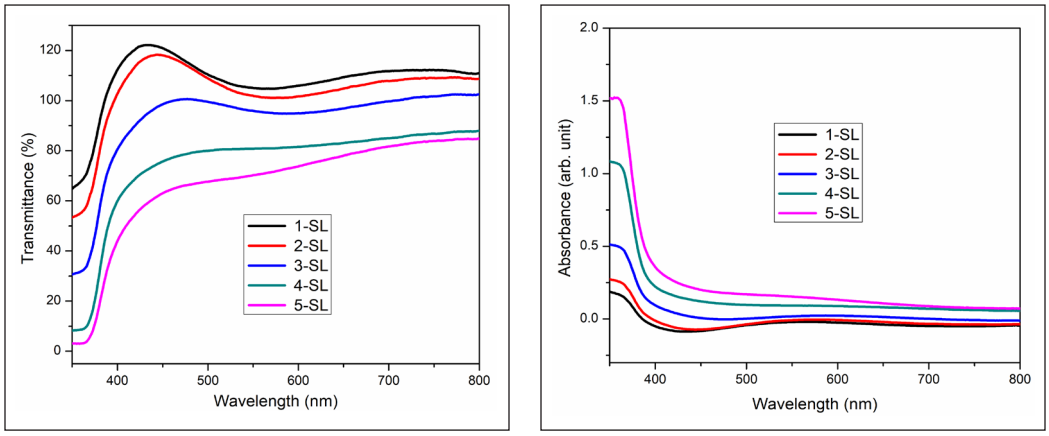

(a) (b)

Figure 7. Optical properties (transmittance and absorbance) for 1-SL, 2-SL, 3-SL, 4-SL, and 5-SL ZnO thin films obtained from UV-Vis

the increment of deposition layers. This difference in *d* values suggests a different value of lattice parameters and atomic radii.

As the deposition layers or number of layers of ZnO thin films was increased, the thickness of the thin films was also increased, as stated earlier. Besides crystallinity, this thickness also affects the optical properties of the deposited ZnO thin films. As shown in Figure 7, the transmittance and absorbance for all samples were measured in the wavelength range between 350–800 nm. Generally, ZnO absorbs in the UV region of the electromagnetic spectrum (Shalu et al., 2020). Based on the transmittance spectra obtained, the transmittance values obtained decrease with the deposition layer of ZnO thin films. It could be related to the thickness of the thin films, which has a linear relationship with the number of layers of ZnO thin films. ZnO thin film with 1-Layer transmits the highest value of transmittance due to the film thickness, which has the lowest value, that allowed the incident light to penetrate easily. Due to this, the transparency of ZnO 1-SL gave the highest value as compared to the other samples. In contrast, ZnO thin film with five layers of deposition gave the lowest transmittance value, caused by the thicker film when further layers were deposited. This thicker layer prevents the incident light penetration for the film with higher thickness. By referring to the thickness value obtained from the surface profilometer, 5-Layer samples have the highest value, which means that there was more interference for incident light to penetrate; thus, the least incident light was transmitted and caused the reduction in transmittance value. This transmittance reduction has satisfied the Beer-Lambert law, given by Equation 9.

$$T = exp^{(-\alpha d)} \quad [9]$$

Where the intensity of transmitted light, *T*, decreases exponentially with the thickness of the sample, *d*, and absorption coefficient, α. As the incident light penetrates and shines through the sample, the total of the incident light reduces due to scattering from the films (Taha et al., 2015). This light scattering might cause the surface roughness and grain size of the films that could be increased from the thickness increment (Teh et al., 2017). The absorbance analysis exposed the light absorption behavior ranging between 350 and 800 nm. Figure 7(b) presents the absorption behavior of all ZnO thin films deposited with 1, 2, 3, 4, and 5 layers. Based on the absorption spectra, the absorbance of all ZnO thin films was proportionally increased with the film thickness. This behavior might be due to the enhancement of the crystallinity quality of the films, which was proved by the XRD analysis obtained. From the UV-Vis measurement, the optical energy band gap for deposited films was estimated and determined using the Tauc relation, given Equation 10.

$$(\alpha hv) = B\left(hv - E_g\right)^n \quad [10]$$

Where α is the absorption coefficient, hv is the photon energy, E_g is the optical bandgap, and B is an energy-independent constant (1×10^5 to 1×10^6 cm^{-1} eV^{-1}), which is dependent on the electron-hole mobility, and n= ½ is used for directly allowed transitions. The calculated optical bandgap for all deposited samples was summarized in Table 4, and the extrapolating graphs are presented in Figures 8(a) to 8(e). The optical energy bandgap is deduced from the intercept of the x-axis at zero y-axes from the plot of αhv against hv through extrapolation of the linear part of the plot. By referring to the calculation results, the increment of optical energy bandgap value for ZnO thin films with a different number of layers could be observed. A slight increment of optical energy band gap was found for each layer that increased. This increasing trend can be related to the crystallinity quality of the thin films. The energy bandgap reduces with the quantum size effect, whereby the bigger the crystal size, the smaller the energy bandgap would obtain (Suzuki et al., 2005). This statement is supported by the crystal size calculated based on XRD spectra, in which the size decreased when a further layer was added. Thus, smaller crystallite size produced a higher value of E_g. Saravanan et al. (2015) also obtained the same trend of optical energy bandgap in their study. In their study, ZnO had been deposited at 20, 50, and 150 nm. They discovered that the optical energy bandgap for their ZnO films increased as the thickness increased, similar to the finding in this study.

Table 4
The value of optical band gap for all ZnO thin films

Number of layers	Optical band gap value (eV)
1	3.15
2	3.19
3	3.21
4	3.24
5	3.25

Next is the investigation of the effect of the ZnO SL thickness on the ZNR growing

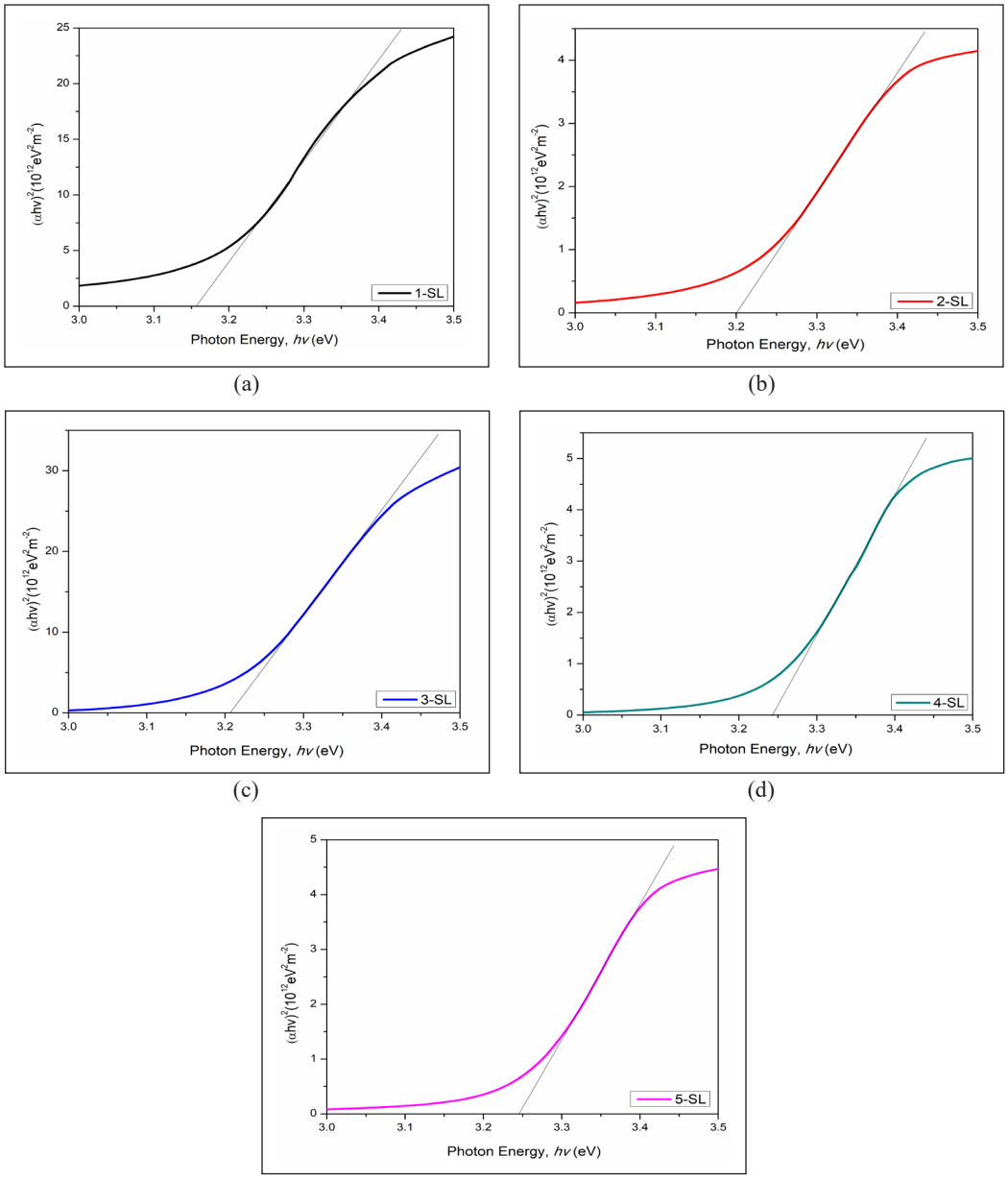

Figure 8. The TAUC plot for estimation of the optical energy band gap, E_g value for all samples (a) 1-SL, (b) 2-SL, (c) 3-SL, (d) 4-SL, and (e) 5-SL

process. As described in the methodology section, the growing process and conditions were constant for all samples. Figures 9(a) to 9(c) shows the morphology for ZNR grown on 1, 3, and 5-layers ZnO thin films observed with FESEM. From the FESEM images, the structures of ZNR improved as the number of layers increased. For 1-Layer SL, irregular

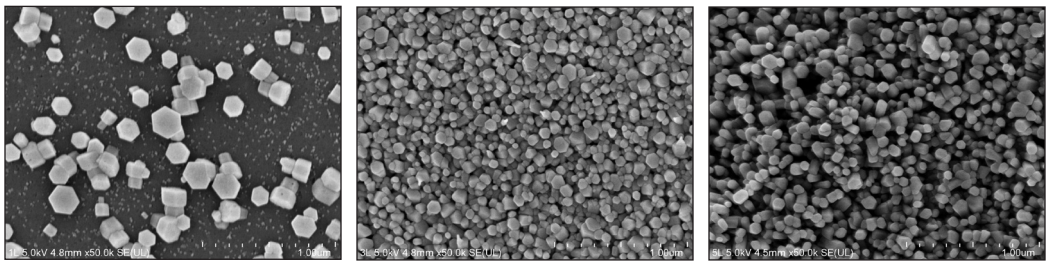

(a) (b) (c)

Figure 9. ZNR structures improved with the increasing number of layers, (a) 1-Layer ZnO SL, (b) 3-Layers SL, and (c) 5-Layers ZnO SL

nanorods were grown on the SL, as shown in Figure 9(a). Even though very sharp hexagonal nanorod structures were observed, the growth of the nanostructures was not uniform, and a large diameter could also observe. This uneven growth might be due to the particles of the ZnO, which were not evenly spread during the deposition process for the 1-Layer ZnO thin film. As explained earlier, the ZnO particles' distribution was improved when a further layer was deposited. The uniformity of the SL is important to produce aligned and dense ZNR because this SL will become the nuclei site for the ZNR to grow.

Significant changes in structures presented in Figures 9(b) and 9(c), 3, and 5 layers of ZnO SL were used to grow ZNR. Uniform and dense ZNR nanostructures grown on both 3 and 5-Layers SL. The enhancement of the growth of ZNR was attributed to the uniform ZnO SL produced when a further layer was added. For example, there might be an uneven distribution of ZnO particles during the first layer. Then another layer was added, and that area was covered; thus, the uniform surface of the nuclei site was produced. A uniform nuclei site would assist the growth of ZNR since the nanorods will grow based on the nuclei site. As a result, uniform and dense ZNR was produced. Similar phenomena were reported by Ikizler et al. (2014). They claimed that the surface seed of the parental seeds could serve as nuclei for the further growth of nanorods.

The surface topology and roughness of the ZNR samples were observed and compared. From the observation, the surface roughness for all samples has a proportional relationship with the thickness value, similar condition with the seed layer. Compared with the seed layer samples, ZNR exhibits a significant increment. The value of the surface roughness ranges from 6.53~70.82 nm. ZNR grown on 5-layers of seed layers gave the roughest surface, which is 70.82 nm. The gradually increasing trend of ZNR surface roughness might be due to the growing process has undergone several processes: nucleation, crystal, and grain growth. Since the ZNR was grown on the seed layer, the last sample (5-SL) produced the roughest surface due to the agglomeration, as shown from FESEM images. From this finding, the 5-SL sample could be a potential candidate for solar cell application due to the highest surface roughness among all prepared samples. The light-trapping process would be more effective on the rougher surface due to the different directions from the surface.

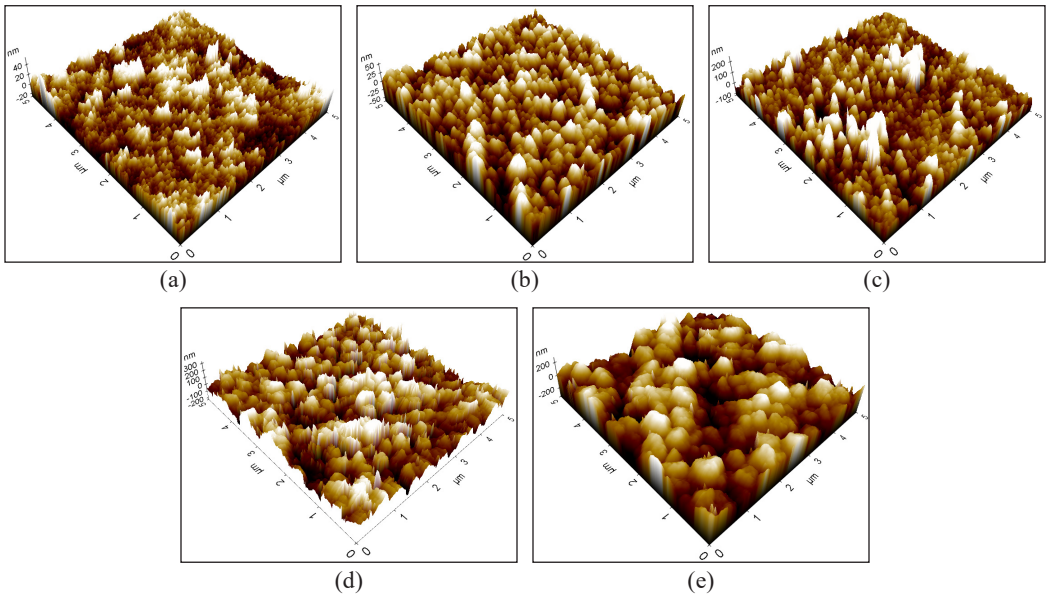

Figure 10. AFM images of the ZNR thin film with (a) 1-layer, (b) 2-layers, (c) 3-layers, (d) 4-layers, and (e) 5-layers seed layer

Scattered light beams will fall on the interfaces non-perpendicularly, which results in higher angular-dependent reflectance at the interfaces compared than in the case of the normal incidence (Lubomir et al., 2014).

The existences of the ZNR crystal structure grown on different numbers of SL were analyzed using XRD measurement, as shown in Figure 10. The variations of crystalline structure for all samples were evident in the XRD patterns, and three major diffraction peaks can be seen. These three diffraction peaks were identified as (100), (002), and (101), which indicates the good crystalline quality of ZNR films prepared. These corresponding peaks are commonly reported peaks for ZnO nanorods structures. Among these three peaks, the (002) peak represents the structural properties of ZnO in the c-direction, the nanorods' growth direction due to the plane's minimum energy. Therefore, the presence of the (002) peak in all samples indicates that the growth direction of ZNR is in perfect alignment (Hock et al., 2016).

It is also can be seen that the intensity of the (100), (002), and (101) plane increase as the thickness of the SL increase. The increasing intensity might be due to the SL's thickness, which affects crystalline quality. On the other hand, it could be related to the SL's thickness, which increases proportionally with the number of layers and improves the crystalline quality of ZnO SL. Due to this, the crystallinity of ZNR was also improved and led to higher peak intensity. Pokai et al. (2016) stated that the cumulative energy on the ZnO surface would increase when the ZnO SL is increased, thus will resulting in high crystallinity of ZnO SL. This finding also can be supported by the morphology obtained

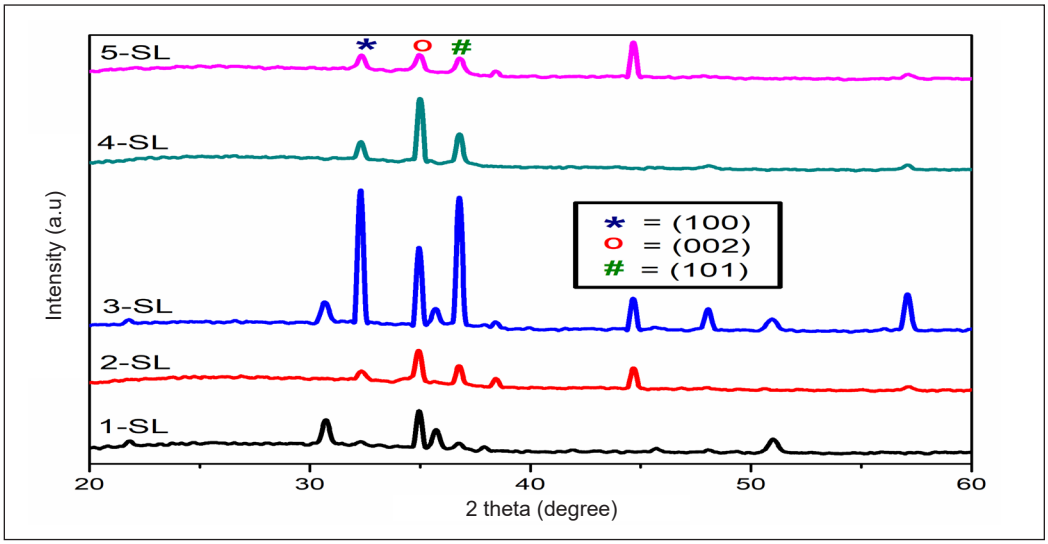

Figure 11. XRD patterns of ZNR grow on different numbers of SL (1, 2, 3, 4, and 5-layers)

by FESEM images. The distribution and growth of ZnO nanorods enhanced with the increase of SL number.

However, the increasing trend of peak intensity started to decrease when 4 and 5 layers were deposited for the SL. It means that ZNR grows at 3-Layers and has the highest intensity for (100), (002), and (101) planes. Notable decrement changes can be seen when the fourth layer was deposited and continue to decrease when the fifth layer was added. The occurrence may cause by the misalignment of the ZnO nanorods during the growth process. It could be explained by the seed/rod number ratio in forming a single rod. As correlated with the morphology of ZNR, misalignment could happen when there are multiple nanorods growing on a single seed. This growth process may lead to the misalignment of a rod, thus affecting the crystallinity of ZnO nanorods. This finding is supported by the study by Ikizler et al. (2014), which also obtained the same finding when the thickness of the SL increases.

From the XRD spectra, full width at half maximum (FWHM), the crystallite size (D), dislocation density (δ), and interplanar spacing (d) were calculated for (100), (002), and (101) planes, while lattice constant (C_{002}) and (a_{100}) were calculated by referring to (002) and (100) planes, respectively. Strain, ε_{zz}, and stress, σ were also calculated and tabulated in Table 5. D, δ, and d were calculated using Equations 6, 7, and 8, as explained earlier for ZnO thin film (seed layer). FWHM, D, δ, and d values for ZNR films decreased as layers increased. However, these values started to rise again for the 4 and 5-Layers samples. The differences in crystallite size may cause the broadening of XRD peaks (Madhavi et al., 2019). It could be proved from the XRD spectra in Figure 11 5-Layers sample has a broader peak compared with the 3 and 4-Layers samples. Other than that, there are reported studies that state that the variation in crystallite is due to the aggregation and

recrystallization during the crystal growth process, including heat structure (McGinty et al., 2020; Padmanabhan et al., 2020).

While for the lattice constant *a* and *c*, the values were obtained by Equations 11 and 12.

$$a = \frac{\lambda}{\sqrt{3}\sin\theta} \quad [11]$$

$$c = \frac{\lambda}{\sin\theta} \quad [12]$$

Here, λ is the constant value of wavelength for the X-ray radiation source (0.154 Å), and θ is the value obtained from 2θ in the spectra. In this study, both *a* and *c* values for all ZNR films are 2.918~3.202 for *a* and 5.112~5.127 for *c*, which approaches the theoretical value of a (3.249) and *c* (5.204). These values also prove that the ZNR films produced in this study have a hexagonal wurtzite structure. As for the strain, ε_{zz}, and stress, σ, the values were calculated based on Equations 13 and 14.

$$\varepsilon_{zz} = \frac{c_{film} - c_{bulk}}{c_{bulk}} \times 100\% \quad [13]$$

$$\sigma = \frac{2C_{13}^2 - C_{33}(C_{11} + C_{12})}{2C_{13}}\,\varepsilon_{zz} \quad [14]$$

For Equation 13, C_{film} signifies the lattice parameter of the ZnO nanorod films, and C_{bulk} is the unstrained lattice parameter for bulk ZnO (5.2066 Å). According to the Equation 14 which used to calculate the stress, C_{ij} is the elastic stiffness constant of bulk ZnO (C_{11}=208.8 GPa, C_{12}=119.7 GPa, C_{13}=104.2 GPa, and C_{33}=213.8 GPa) and ε_{zz} is the lattice strain obtained from Equation 13. The difference in film thickness had affected the crystal growth, including the formation of strain and stress in the lattice (Chason et al., 2018). The positive and negative strain values represent the tensile strain when the film is stretched and the compressive strain when compressed (Chason et al., 2018). In short, the positive value could be classified as a tensile strain; in contrast, it is considered a compressive strain. While for stress, if the value obtained is positive, it is considered tensile stress, and the negative value indicates the compressive stress [49–50]. Therefore, based on the calculation, the strain values for ZNR films in this study were obtained in a negative value, which is compressive strain. This phenomenon could be related to the film's crystallite size, decreasing as the thickness increases. Rezaie et al. (2018) reported that the increase in film thickness might be promoted by decreasing crystallite size because bigger crystallite size may induce lower-strained films. Moreover, the reduction of crystallite size and film strain enhancement was supported by the decreased *d* and c_{film} values obtained. In contrast with stress, the values were positive, representing the tensile stress.

The difference in strain and stress of ZNR films might be attributed to deficiencies in the crystal's lattice, such as stacking faults, grain boundaries, and dislocation density (Irvine et al., 2013). Usually, the grain boundary formation is believed to develop the strain and stress of the films. The interactions between the grains would lead to the tensile stress, while adding an adatom into the grain boundaries causes compressive stress (Yang et al., 2019). Meanwhile, the growth rate and atom surface mobility could be related to their strain and stress magnitudes (Magnfalt et al., 2015). Stresses might occur in the grown film that used the aqueous solution approach during the fabrication process, resulting in a lattice strain. Compressive tensile may occur during the growth process; thus, the strain and stress are determined by the growth parameters.

Table 5
2θ, FWHM, crystallite size, dislocation density, interplanar spacing, lattice constant, strain and stress of ZNR grow on different number of SL

Samples	Orientation, hkl	2θ (°)	FWHM	Crystallite size, D (nm)	Dislocation line density, δ (δ x 10-3 line/nm2)	Interplanar spacing, d (Åm)	Lattice constant		Strain, ε_{zz} (%)	Stress , σ, (GPa)
							a_{100}	c_{002}		
	100	32.35	0.4497	32.86	0.926	2.7677				
1-SL	002	34.97	0.3695	40.00	0.625	2.5668	3.190	5.127	-1.5307	3.56
	101	36.83	0.4675	31.61	1.000	2.4404				
	100	32.35	0.4042	32.35	0.748	2.7674				
2-SL	002	34.97	0.3413	34.97	0.534	2.5665	2.918	5.126	-1.5480	3.60
	101	36.74	0.3348	36.74	0.513	2.4468				
	100	32.24	0.3001	32.25	0.414	2.7764				
3-SL	002	34.97	0.1544	34.97	0.109	2.5665	3.202	5.127	-1.5480	3.60
	101	36.74	0.3087	36.74	0.436	2.4468				
	100	32.36	0.3295	44.83	0.498	2.7670				
4-SL	002	35.06	0.3062	48.26	0.429	2.5594	3.191	5.112	-1.8131	4.22
	101	36.75	0.3499	42.22	0.561	2.4467				
	100	32.35	0.3745	39.43	0.643	2.7674				
5-SL	002	35.06	0.4019	36.77	0.740	2.5594	3.193	5.112	-1.8150	4.22
	101	36.83	0.4406	33.53	0.889	2.4403				

The variations in the crystalline quality and lattice properties of the ZNR films may contribute to the variation and changes in the optical properties of fabricated ZNR samples. Fig. 12 (a) and (b) represent all samples' transmittance and absorbance analyses, ranging between 350-800 nm, respectively. The transmittance of the ZnO nanorods grown shows a high percentage of transparency, in the range of 30~95% in the visible range. The range of the transparency value for ZNR films is slightly lower than for ZnO thin films. Fabricated films become thicker when ZNR is grown on the ZnO thin film, resulting in a

lower transparency value of ZNR films. As described in Figure 12(a), the transmittance of ZNR films shows a decrement trend with the increment of several layers due to the higher absorption capacity of thicker films. The least transparency value in the thicker film might be reasoning to the thick layer, which prevents the incident light from penetrating through the layer. Other than that, the percentage of transmittance would reduce in the UV region due to the onset of excitonic absorption (Ikizler & Peker, 2014).

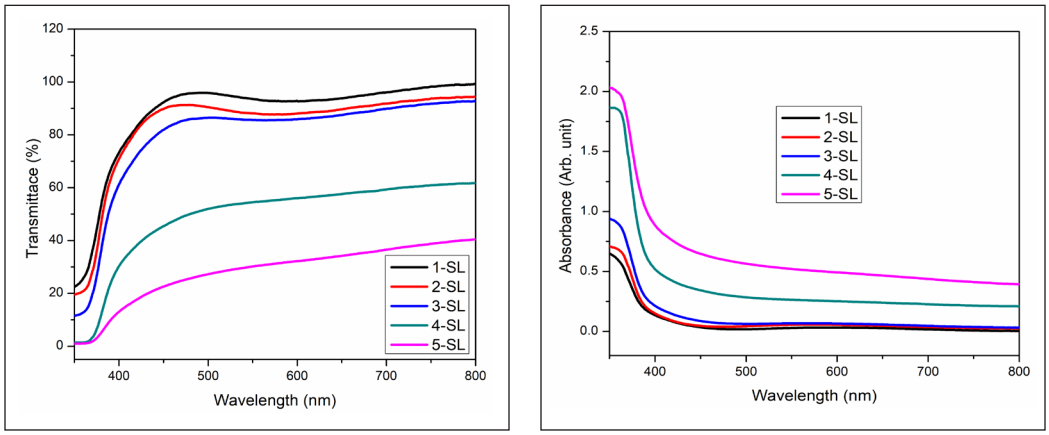

(a) (b)

Figure 12. (a) Transmittance and (b) Absorbance spectra for ZNR films grown on different numbers of SL

As for the optical absorbance, the absorption properties of the ZNR films with different numbers of SL increase proportionally to the SL numbers in the UV region (below 400 nm) and lower in the visible region (400–800 nm). The result shows that ZnO nanorods grown on 5-Layers of SL show maximum UV absorbance value. This finding corresponds to the optical energy bandgap, calculated referring to eq. (10). The E_g values for all ZNR samples are presented in Table 6. The E_g values for all samples were estimated from the intercept of the x-axis, and the plot for all samples is shown in Figure 13. From Tauc's plot, the E_g of ZNR films has a directly proportional relationship with the number of layers of SL. This increment occurs due to the film's thickness that increases when the SL number increases. Therefore, the increasing number of layers would produce a thicker film, which influences the transmittance, absorbance, and optical energy band gap.

The increase in grain size and strain might cause the increment in band gap value (Ikizler & Peker, 2014). In addition, this grain size will increase if the thickness or chemical composition increases. These two

Table 6
Optical energy bandgap for ZnO nanorods sample grown on a various number of SL

Sample	Optical band gap value (eV)
1-SL	3.23
2-SL	3.27
3-SL	3.28
4-SL	3.29
5-SL	3.67

factors will directly change the material (thin film) band gap (El Zawawi et al., 2017). Therefore, even though the same material was used, the optical energy band gap would change significantly with thickness and chemical composition changes. Other than that, crystallinity, temperature, particle size, and a few other factors will also affect the value of the energy band gap of thin film (Mahato et al., 2017).

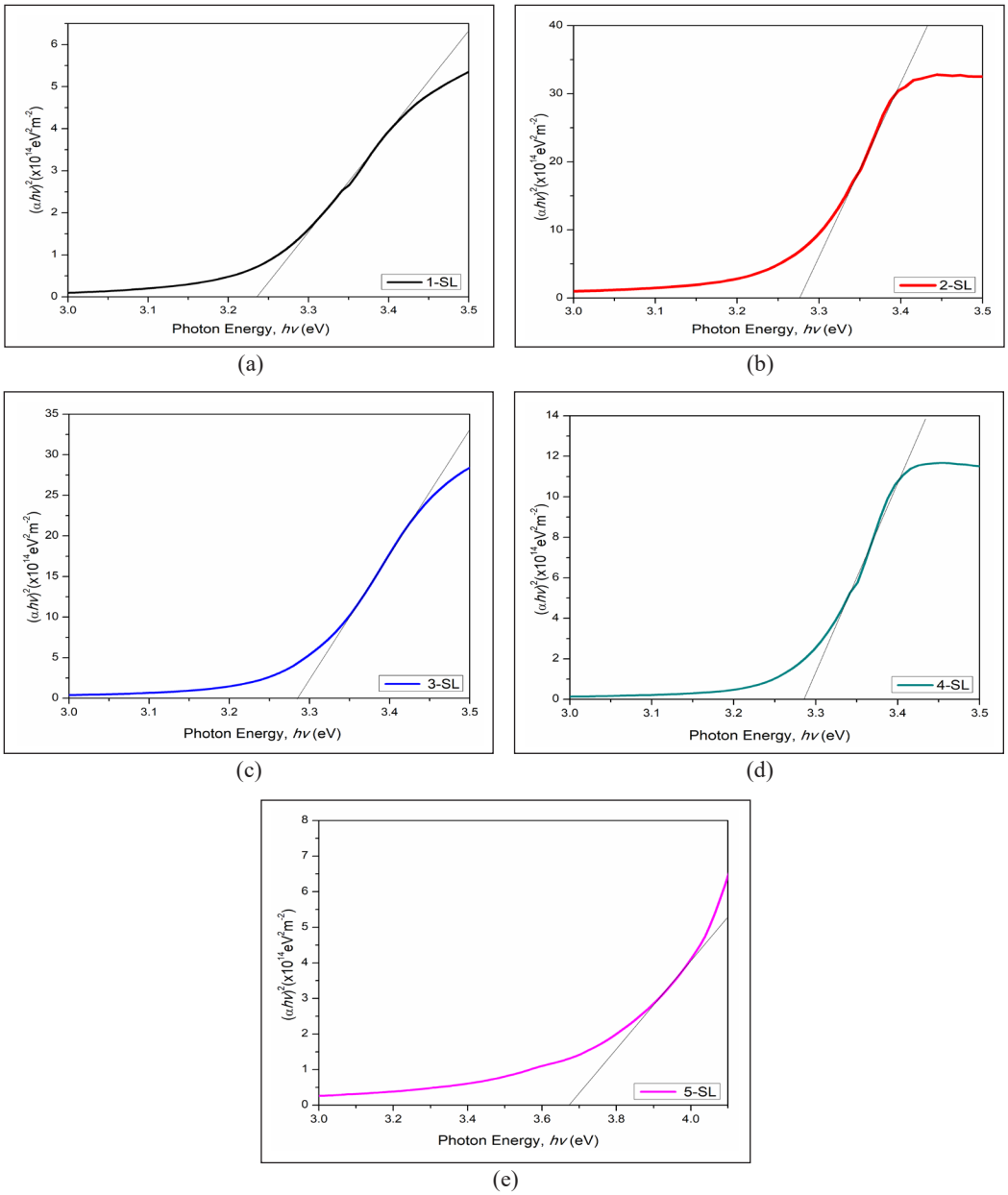

Figure 13. Estimation of E_g for ZNR grown on (a) 1-SL, (b) 2-SL, (c) 3-SL, (d) 4-SL, and (e) 5-SL of a seed layer

CONCLUSION

In conclusion, multilayer ZnO thin film and well-aligned ZNR films were successfully synthesized using the sol-gel spin coating technique and chemical bath deposition methods. From the results obtained, it was found that the thickness of the films could influence the characteristics and properties of the fabricated ZnO films. Increasing the thickness of ZnO thin film that functions as the SL for ZNR growth influenced the structure and orientation of ZNR. For consideration of morphology ZNR, the images obtained revealed that 5-layers ZnO SL produced well-aligned and dense-packed ZNR. It was evident that the crystalline quality and optical properties of ZnO and ZNR films were also improved by the increment of the thickness of the SL. XRD analysis shows that all ZNR samples exhibit (100), (002), and (101) peaks, which prove that the films have good crystalline quality. Also, AFM analysis revealed that higher thickness of the seed layer produced rougher surface ZNR, which is one of the characteristics of the good potential for a solar cell.

ACKNOWLEDGEMENT

The authors want to thank all members of Nano Electronic Center (NET), Integrated Sensors Research Group (DERIA), and Nano-Science Technology Center (NST, Universiti Teknologi MARA (UiTM) Shah Alam for all the research facilities. In addition, the Ministry of Higher Education Malaysia partially supports this work under the Fundamental Research Grant Scheme (FRGS/1/2017/TK04/UITM/02/16).

REFERENCES

Abdel-Galil, A., Hussien, M. S., & Yahia, I. S. (2021). Synthesis & optical analysis of nanostructures F-doped ZnO thin films by spray pyrolysis: Transport electrode for photocatalytic applications. *Optical Materials, 114*, Article 110894. https://doi.org/10.1016/j.optmat.2021.110894

Abdulrahman, A. F., Ahmed, S. M., Ahmed, N. M., & Almessiere, M. A. (2020). Enhancement of ZnO nanorods properties using modified chemical bath deposition method: Effect of precursor concentration. *Crystal*, *10*(5), Article 386. https://doi.org/10.3390/cryst10050386

Addamo, M., Augigliaro, V., Di Paola, A., Garcia-Lopez, E., Loddo, V., Marci, G., & Palmisano, L. (2008). Photocatalytic thin films of TiO_2 formed by sol-gel process using titanium tetraisopropoxide as the precursor. *Thin Solid Films, 516*(12), 3802-3807. https://doi.org/10.1016/j.tsf.2007.06.139

Al Farsi, B., Souier, T. M., Al Marzouqi, F., Al Maashani, M., Bououdina, M., Widatallah, H. M., & Al Abri, M. (2021). Structural and optical properties of visible active photocatalytic Al doped ZnO nanostructured thin films prepared by dip coating. *Optical Materials*, *113*, Article 110868. https://doi.org/10.1016/j.optmat.2021.110868

Alenezi, M. R. (2018). Hierarchical zinc oxide nanorings with superior sensing properties. *Materials Science and Engineering: B, 236*(237), 132-138. https://doi.org/10.1016/j.mseb.2018.11.011

Banari, M., Memarian, N., & Vomiero, A. (2021). Effect of the seed layer on the photodetection properties of ZnO nanorods. *Materials Science and Engineering: B*, *272*, Article 115332. https://doi.org/10.1016/j.mseb.2021.115332

Bindu, P., & Thomas, S. (2014). Estimation of lattice strain in ZnO nanoparticles: X-ray peak profile analysis. *Journal of Theory Applied Physics, 8*, 123-134. https://doi.org/10.1007/s40094-014-0141-9

Chason, E., Keckes, J., Sebastian, M., Thompson, G. B., Barthel, E., Doll, G. L., Murray, C. E., Stoessel, C. H., & Martinu, L. (2018). Review articles: Stress in thin films and coatings: Current status, challenges, and prospects. *Journal of Vacuum Science and Technology A*, *36*(2), 1-49. https://doi.org/10.1116/1.5011790

Chen, X. X., Chen, L., Li, G., Cai, L. X., Miao, G., Guo, Z., & Meng, F. L. (2021). Selectively enhanced gas-sensing performance to n-butanol based on uniform CdO-decorated porous ZnO nanobelts. *Sensors and Actuators B: Chemical, 334*, Article 129667. https://doi.org/10.1016/j.snb.2021.129667

Daniel, L., Falko, S., & Dietrich, R. Z. (2014). Thin films woth high surface roughness: Thickness and dielectric function analysis using spectroscopic ellipsometry. *Methodology, 3*(82), 1-8. https://doi.org/10.1186/2193-1801-3-82

Djurisic, A. B., Ng, A. M. C., & Chen, X. Y. (2010). ZnO nanostructures for optoelectronics: Material properties and device applications. *Progress in Quantum Electronics*, *34*(4), 191-259. https://doi.org/10.1016/j.pquantelec.2010.04.001

El Zawawi, I. K., Mahdv, M. A., & El-Sayad, E. A. (2017). Influence of film thickness and heat treatment on the physical properties of Mn doped Sb_2Se_3 nanocrystalline thin films. *Journal of Nanomaterials, 2017*, Article 7509098. https://doi.org/10.1155/2017/7509098

Gonçalves, R. S., Barrozo, P., Brito, G. L., Viana, B. C., & Cunha, F. (2017). The effect thickness on optical, structural, and growth mechanism of ZnO thin film prepared by magnetron sputtering. *Thin Solid Films*, *661*, 40-45. https://doi.org/10.1016/j.tsf.2018.07.008

Gunes, S., Neugebauer, H., & Sariciftci, N. S. (2007). Conjugated polymer-based organic solar cells. *Chemical Reviews, 107*(4), 1324-1338. https://doi.org/10.1021/cr050149z

Hajezi, S. R., Hosseini, H. M., & Ghamsari, M. S. (2008). The role of reactants and droplet interfaces on nucleation and growth of ZnO nanorods synthesized by vapor-liquid-solid (VLS) mechanism. *Journal of Alloys and Compounds*, *455*(1-2), 353-357. https://doi.org/10.1016/j.jallcom.2007.01.100

Hasabeldaim, E. H. H., Ntwaeborwa, O. M., Kroon, R. E., Coetsee, E., & Swart, H. C. (2020). Luminescence properties of Eu doped ZnO PLD thin films: The effect of oxygen partial pressure. *Superlattices and Microstructures*, *139*, Article 106432. https://doi.org/10.1016/j.spmi.2020.106432

Hock, B. L., Riski, T. G., Sin, T. T., Chun, H. T., Alshanableh, A., Oleiwi, H. F., Chi, C. Y., Hj Jumali, M. H., & Muhammad Yahaya. (2016). Controlled defect fluorine-incorporated ZnO nanorods for photovoltaic enhancement. *Scientific Reports, 6*, Article 32645. https://doi.org/1-11.10.1038/srep32645

Huey, J. T., Zainal, Z., Talib, Z. A., Hong, N. L., Shafie, S., Sin, T. T., Kar, B. T., & Bahrudin, N. N. (2021). Synthesis of high quality hydrothermally grown ZnO nanorods for photoelectrochemical cell electrode. *Ceramics International*, *47*(10, Part A), 14194-14207. https://doi.org/10.1016/j.ceramint.2021.02.005

Ikizler, B., & Peker, S. M. (2014). Effect of the seed layer thickness on the stability of ZnO nanorod arrays. *Thin Solid Film*, *558*, 149-159. https://doi.org/10.1016/j.tsf.2014.03.019

Irvine, W. T. M., Hollingsworth, A. D., Grier, D. G., & Chaikin, P. M. (2013). Dislocation reactions, grain boundaries, and irreversibility in two-dimensional lattices using topological tweezers. *Applied Physical Sciences*, *110*(39), 15544-15548. https://doi.org/10.1073/pnas.1300787110

Jimenez-Cadena, G., Comini, E., Ferroni, M., Vomiero, A., & Sberveglieri, G. (2010). Synthesis of different ZnO nanostructures by modified PVD process and potential use for dye-sensitized solar cells. *Materials Chemistry and Physics, 124*(1), 694-698. https://doi.org/10.1016/j.matchemphys.2010.07.035

Kaiyong, C., Michael, M., Korg, B., Annett, R., & Klaus, D. J. (2005) Surface structure and composition of flat titanium thin films as a function of film thickness and evaporation rate. *Applied Surface Science, 250*(2005), 252-267. https://doi.org/10.1016/j.apsusc.2005.01.013.

Kamalianfar, A., Halim, S. A., Behzad, K., Naseri, M. G., Navasery, M., Din, F. U., Zahedi, J. A. M., Lim, K. P., Chen, S. K., & Sidek, H. A. A. (2013) Effect of thickness on structural, optical, and magnetic properties of Co doped ZnO thin film by pulsed laser deposition. *Journal of Optoelectronics and Advanced Materials, 15*(3), 239- 243.

Kannan, S., Subiramaniyam, N. P., & Lavanisadevi, S. U. Controllable synthesis of ZnO nanorods at different temperatures for enhancement of dye-sensitized solar cell performance. *Material Letters, 274*, Article 127994. https://doi.org/10.1016/j.matlet.2020.127994

Khan, M. I., Bhatti, K. A., Alonizan, N., & Althobaiti, H. S. (2017). Characterization of multilayer ZnO thin films deposited by sol-gel spin coating technique. *Results in Physics, 7*, 651-655. https://doi.org/10.1016/j.rinp.2016.12.029

Khan, Z. R., Abdullah S. Alshammari., Bouzidi, M., Shkir, M., & Shukla, D. K. (2021). Improved optoelectronic performance of sol-gel derived ZnO nanostructured thin films. *Inorganic Chemistry Communications, 132*, Article 108812. https://doi.org/10.1016/j.inoche.2021.108812

Khranovskyy, V., Yakimova, R., Karlsson, F., Abdul, S. S., Holtz, P., Urgessa, Z. N., Oluwafemi, O. S., & Botha, J. R. (2012). Comparative PL study of individual ZnO nanorods, grown by APMOCVD and CBD technique. *Physica B: Condensed Matter*, *407*(10), 1538-1442. https://doi.org/10.1016/j.physb.2011.09.080

Kumar, S., Share, P. D., & Kumar, S. (2018). Optimization of CVD parameters for ZnO nanorods growth: Its photoluminescence and field emission properties. *Materials Research Bulletin*, *105*, 237-245. https://doi.org/10.1016/j.materresbull.2018.05.002

Kumar, V., Singh, N., Mehra, R. M., Kapoor, A., Purohit, L. P., & Swart, H. C. (2013). Role of film thickness on the properties of ZnO thin films grown by sol-gel method. *Thin Solid Films*, *539*. https://doi.org/10.1016/j.tsf.2013.05.088

Lokesh, K. S., Kumar, J. R. N., Kannantha, V., Pinto, T., & Sampreeth, U. (2020). Experimental evaluation of substrate and annealing conditions on ZnO thin films prepared by sol-gel method. *Materialstoday: Proceedings, 24*(2), 201-208. https://doi.org/10.1016/j.matpr.2020.04.268

Lubomir, S., Libor, L., & Jarmila, M. (2014). Influence of surface roughness on optical characteristics of multilayer solar cells. *Applied Physics, 12*(6), 631-64. 10.15598/aeee.v12i6.1078

Madhavi, J. (2019). Comparison of average crystallite size by X-ray peak broadening and Williamson-Hall and size-strain plots for VO^{2+} doped ZnS/CdS composite nanopowder. *SN Applied. Science, 1*, Article 1509. https://doi.org/10.1007/s42452-019-1291-9

Magnfalt, D., Fillon, A., Boyd, R. D., Helmersson, U., Sarakinos, K., & Abadias, G. (2015). Compressive intrinsic stress originates in the grain boundaries of dense refractory polycrystalline thin films. *Journal of Applied Physics*, *119*(5), Article 055305. https://doi.org/10.1063/1.4941271

Mahato, S., & Kar, A. K. (2017). The effect of annealing on structural, optical, and photosensitive properties of electrodeposited cadmium selenide thin films. *Journal of Science: Advanced Materials and Devices*, *2*(2), 165-171. https://doi.org/10.1016/j.jsamd.2017.04.001

McGinty, J., Yazdanpanah, N., Price, C., Joop, H. T., & Sefcik, J. (2020). Nucleation and crystal growth in continuous crystallization. In N. Yazdanpanah & Z. K. Nagy (Eds.), *The Handbook of Continuous Crystallization* (pp. 1-50). Royal Society of Chemistry. https://doi.org/10.1039/9781788013581-00001

Mohammadzadeh, A., Azadbeh, M., Shokriyan, B., & Abad, S. N. K. (2020). Synthesis of ZnO nanocombs and tetrapods by catalyst-free oxidation of alpha brass powders in air atmosphere. *Ceramics International*, *46*(2), 2552-2557. https://doi.org/10.1016/j.ceramint.2019.09.112

Mosalagae, K., Murape, D. M., & Lepodise, L. M. (2020). Effects of growth conditions on properties of CBD synthesized ZnO nanorods grown on ultrasonic spray pyrolysis deposited ZnO seed layers. *Heliyon*, *6*(7), 1-10. https://doi.org/10.1016/j.heliyon.2020.e04458

Padmanabhan, S. C., Collins, T. W., Pillai, S. C., McCormack, D. E., Kelly, J. M., Holmes, J. D., & Morris, M. A. (2020). A conceptual change in crystallisation mechanisms of oxide materials from solutions in closed systems. *Scientific Reports, 10,* Article 18414. https://doi.org/10.1038/s41598-020-75241-z

Pokai, S., Lomnonthakul, P., Horprathum, M., Kalasung, S., Eiamchai, P., Limwichean, S., Nuntawong, N., Pattantsetakul, V., Tuscharoen, S., & Kaewkhao, J. (2016). Influence of growth conditions on morphology of ZnO nanorods by low-temperature hydrothermal method. *Key Engineering Materials*, *675-676*, 53-56. https://doi.org/10.4028/www.scientific.net/kem.675-676.53

Regmi, G., & Velumani, S. (2021). Impact of target power on the properties of sputtered intrinsic zinc oxide (i-ZnO) thin films and its thickness dependence performance on CISE solar cells. *Optical Materials*, *119*, Article 111350. https://doi.org/10.1016/j.optmat.2021.111350

Rezaie, M. N., Manavizadeh, N., Nayeri, F. D., Bidgoli, M. M., Nadimi, E., & Boroumand, F. A. (2018). Effect of seed layers on low-temperature, chemical bath deposited ZnO nanorods-based near UV-OLED performance. *Ceramics International*, *44*(5), 4937-4945. https://doi.org/10.1016/j.ceramint.2017.12.086

Rodriguez-Martinez, Y., Alba-Cabarnas, J., Cruzata, O., Bianco, S., Tresso, E., Rossi, F., & Vaillant-Roca, L. (2020). In-situ pulsed laser induced growth pf CdS nanoparticles on ZnO nanorods surfaces. *Material Research Bulletin, 125*, Article 110790. https://doi.org/10.1016/j.materresbull.2020.110790

Roy, S., Banerjee, N., Sarkar, C. K., & Bhattacharyya, P. (2013). Development of an ethanol sensor based grown ZnO nanorods. *Solid-State Electronics, 87*, 43-50. https://doi.org/10.1016/j.sse.2013.05.003

Rwenyagila, E. R., Ayei-Tuffour, B., Kana, M. G. Z., Akin-Ojo, O. & Soboyejo, W. O. (2014). Optical properties of ZnO/Al/ZnO multilayer films for large area transparent electrodes. *Journal of Material Research*, *29*, 2912-2920. https://doi.org/10.1557/jmr.2014.298

Saravanan, K., Krishnan, R., Hsieh, S. H., Wang, H. T., Wang, Y. F., Pong, W. F., Asokan, K., Avasthi, D. K., & Kanjilal, D. (2015). Effect of defects and film thickness on the optical properties of ZnO-Au hybrid films. *Royal Society of Chemistry Advances*, *51*(5), 40813-40820. https://doi.org/10.1039/c5ra02144h

Scholtz, L., Ladanyi, L., & Mullerova, J. (2014). Influence of surface roughness on optical characteristics of multilayers solar cells. *Applied Physics*, *12*(6), 631-640. https://doi.org/10.15598/aeee.v12i6.1078

Shalu, G., Shukla, M., Tiwari, A., Agrawal, J., Bilgaiyan, A., & Singh, V. (2020). Role of solvent used to cast P3HT thin films on the performance of ZnO/P3HT hybrid photo detector. *Physica E: Low-dimensional Systems and Nanostructures*, *115*, Article 113694. https://doi.org/10.1016/j.physe.2019.113694

Shariffudin, S. S., Salina, M., Herman, S. H., & Rusop, M. (2012). Effect of film thickness on structural, electrical, and optical properties of sol-gel deposited layer-by-layer ZnO nanoparticles. *Transaction on Electrical and Electronic Materials, 13*(2), 102-105. https://doi.org/10.4313/TEEM.2012.13.2.102

Sharma, S., Vyas, S., Periasamy, C., & Chakrabarti, P. (2014). Structural and optical characterization of ZnO thin films for optoelectronic device applications by RF sputtering technique. *Superlattices and Microstructures, 75*, 378-389. https://doi.org/10.1016/j.spmi.2014.07.032

Suzuki, K., & Kijima, K. (2005). Optical band gap of barium titanate nanoparticles prepared by RF-plasma chemical vapor deposition. *Japanese Journal of Applied Physics*, *44*(4R), 2081-2082. https://doi.org/10.1143/JJAP.44.2081

Taha, K. K., M'hamed, M. O., & Idris, H. (2015). Mechanical fabrication and characterization of zinc oxide (ZnO) nanoparticles. *Journal of Ovonic Research*, *11*(6), 271-276.

Teh, Y. C., Ala'eddin, A. S., Jamal, Z. A. Z., & Poopalan, P. (2017). Correlation of film thickness to optical band gap of sol-gel derived $Ba_{0.9}Gd_{0.1}$ TiO_3 thin films for optoelectronic applications. *EPJ Web of Conferences*, *162,* Article 01042. https://doi.org/10.1051/epjconf/201716201042

Yang, G., & Park, S. J. (2019). Deformation of single crystal, polycrystalline materials, and thin films: A review. *Materials, 12*(12), 1-18. https://doi.org/10.3390/ma12122003

Zhang, Y., Ram, M. K., Stefanakos, E. K., & Goswami, D. Y. (2012). Synthesis Characterization, and application of ZnO nanowires. *Nanofiber Manufacture, Properties and Application*, *2012*, Article 624520. https://doi.org/10.1155/2012/624520

Zhou, L., Zeng, W., & Li, Y. (2019). A facile one-step hydrothermal synthesis of a novel NiO/ZnO nanorod composite and its enhanced ethanol sensing property. *Material Letters, 254*, 92-95. https://doi.org/10.1016/j.matlet.2019.07.042